Heliyon 9 (2023) e21729

Contents lists available at ScienceDirect

Heliyon

journal homepage: www.cell.com/heliyon

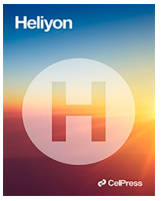

Solid waste filling and roadway retaining for longwall mining by numerical investigation

Kai Sun [a,b], Yongjin Huo [a,b], Jian Li [c,*], Fei Guo [a,b], Yinghao Hao [a,b], Gang Bai [a,b], Yuyi Wu [a,d], Xiaofang Wo [c]

[a] China National Coal Group Corporation, Beijing, 100120, China
[b] Coal Branch, Zhongtianhechuang Energy Co., Ltd. Ordos, Inner Mongolia, 017000, China
[c] School of Mines, Key Laboratory of Deep Coal Resource Mining, Ministry of Education of China, China University of Mining and Technology, Xuzhou, Jiangsu 221116, China
[d] China Coal Energy Research Institute Co., Ltd, Xi'an, Shaanxi, 710000, China

ARTICLE INFO

Keywords:
Solid waste filling
Green mining
Roadway retaining along goaf
Filling rate
Roof subsidence

ABSTRACT

Solid waste filling and roadway retaining can effectively control surface subsidence and alleviate solid waste accumulation pollution. In order to effectively evaluate the advantages of solid waste filling in deformation control of overlying strata and surrounding rock of retained roadways, this study used theoretical analysis and numerical simulation methods to analyze the factors affecting surface subsidence, as well as the deformation characteristics of surrounding rocks and retaining tunnels during backfill mining. By calculating the influence of factors such as the foundation coefficient and the filling rate on the subsidence of the roof, it is concluded that the filling rate is the main controlling factor affecting the subsidence of the roof. Through simulation and comprehensive analysis of the impact of different filling rates on overlying rock migration, it was found that when the filling rates are 70 % and 80 %, it can effectively control the subsidence of overlying rock in the mining area. By simulating the effects of these two filling rate conditions on the deformation of surrounding rock within the retained roadway zone, the results show that the optimal filling rate that can effectively control the subsidence of the overlying rock and improve the stability of the retained roadway is 80 %.

1. Introduction

Coal mining is associated with a number of environmental problems. On the one hand, coal mining causes the movement and destruction of overlying rock strata, which results in the loss of groundwater and the destruction of surface vegetation [1–3]. On the other hand, some coal mining processes affect the extraction rate of coal resources, resulting in a waste of coal resources [4–7]. The process of coal mining also produces a large amount of coal gangue waste, which accumulates on the surface, occupies good land and pollutes surface water and groundwater [8–12].

Technical bottlenecks in the traditional coal mining field constrain the development of the coal mining field. Many mines have experienced decades of high-intensity mining leading to a surge in mining difficulty [13–15]. The method of leaving large-scale coal pillars in mines not only loses a large amount of coal resources, but also produces stress concentration phenomenon that affects the

* Corresponding author.
E-mail address: lijiancumt10@163.com (J. Li).

https://doi.org/10.1016/j.heliyon.2023.e21729
Received 6 July 2023; Received in revised form 20 October 2023; Accepted 26 October 2023
Available online 4 November 2023

safety of the mines. In order to alleviate the surface subsidence caused by coal mining resources, reduce the environmental problems caused by the accumulation of coal gangue waste, and improve the extraction rate of coal resources, it has become an important technology to combine roadway retaining and solid waste filling process. Many scholars have conducted research on this. Some scholars have analysed the technical difficulties and construction keys of the roadway retaining and solid waste filling [16–19]. Some scholars have analysed the deficiencies of the roadway retaining and solid waste filling technology, and put forward the formation of roadside support by filling gangue belt and grouting reinforcement of filling body [18,20–22]. Therefore, it further improves the deficiency of this technology in deep filling mining conditions [23–26]. Some scholars constructed a structural mechanics model of roadway retaining and backfill mining under the thick hard roof, and analysed that improving the filling rate is the main means of controlling the deformation of the retained roadway [27–29]. Some scholars have proposed a new stable synergistic bearing structure for roadway retaining and backfill mining，which is called “load-bearing rock layer - filling body - roadside support body - coal body”, and analysed the support characteristics of its constituent elements [30].

The objective of this study is to investigate the protective role of coal gangue waste on the rock strata above the goaf and the retained roadway during underground backfilling mining. The research employs theoretical calculation and numerical simulation techniques to examine the factors that influence surface subsidence, the migration behavior of overburden rock, and the deformation characteristics of retained roadways in fill mining [31]. The theoretical calculation confirms the significant impact of the filling rate on controlling roof subsidence. Then, the effects of various filling rates on surrounding rock fragmentation and roof subsidence are analysed by numerical simulation. Ultimately, the study evaluates the impact of the filling rate on the stability of the retained roadways explores the optimal filling rate scheme, which guides the field engineering practice.

2. Project overview

CT21201 of Hulusu Coal Mine is a coal mining face with filling and retaining roadway, which is located in the middle of 2–1 coal panel of Hulusu minefield. The working face is 80 *m* wide, with roadways on each side measuring 5.4 *m* in width. The coal seam is located at a depth of 630~640 *m*, and it has a dip angle ranging from -3° to $+3^\circ$, making it a nearly horizontal coal seam. The average thickness of the coal seam, immediate roof, main roof, immediate floor, and hard floor are 3.2 *m*, 4 *m*, 10 *m*, 8 *m*, and 12 *m*, respectively. Fig. 1 shows the project background map.

3. Mechanical model of gob side entry retaining for filling mining

In order to analyze the main controlling factors of roof subsidence, a mechanical model of backfill mining is established based on the collaborative control method of backfill mining. The coordinate system is established, with the origin located at the intersection point of the filling body's edge and the side support of the roadway. The x-axis is aligned with the inclination direction of the working face, while the y-axis represents the height direction of the roadway. Q is the equivalent uniformly distributed load on the upper part, $k_m y$ represents the support force at the coal wall. $k_z y$ is the support force at the retained roadway. $k_e y$ is the support force for the side support of the roadway. $k_c y$ is the supporting force of the filling body in the goaf. By applying the Winkler hypothesis and taking into account relevant literature, the differential equation for the deflection of rock beams is obtained as shown in Equation (1).

$$y=\begin{cases} e^{\alpha x}[A_1\sin(\alpha x)+A_2\cos(\alpha x)]+e^{-\alpha x}[A_3\sin(\alpha x)+A_4\cos(\alpha x)]+\dfrac{q}{k_m} & x\in(-L_1-L_2-L_3,-L_2-L_3)\\ e^{\beta x}[B_1\sin(\beta x)+B_2\cos(\beta x)]+e^{-\beta x}[B_3\sin(\beta x)+B_4\cos(\beta x)]+\dfrac{q}{k_z} & x\in(-L_2-L_3,-L_3)\\ e^{\delta x}[C_1\sin(\delta x)+C_2\cos(\delta x)]+e^{-\delta x}[C_3\sin(\delta x)+C_4\cos(\delta x)]+\dfrac{q}{k_e} & x\in(-L_3,0)\\ e^{-\gamma x}[D_1\sin(\gamma x)+D_2\cos(\gamma x)]+e^{\gamma x}[D_3\sin(\gamma x)+D_4\cos(\gamma x)]+\dfrac{q}{k_c}+f_c & x\in(0,L_4)\\ e^{-\alpha x}[E_1\sin(\alpha x)+E_2\cos(\alpha x)]+e^{\alpha x}[E_3\sin(\alpha x)+E_4\cos(\alpha x)]+\dfrac{q}{k_m} & x\in(L_4,L_4+L_5) \end{cases} \tag{1}$$

The relationship equation among the rotation angle (x) , bending moment $M(x)$, shear force $Q(x)$, and deflection y is expressed by

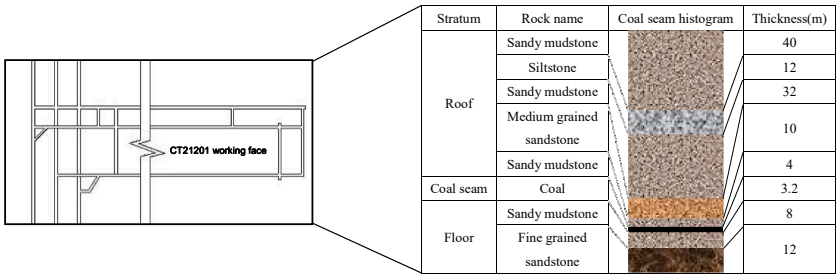

Fig. 1. Project background.

the following equation (2).

$$\begin{cases} \theta(x) = \dfrac{dy}{dx} \\ M(x) = -EI\dfrac{d^2y}{dx^2} \\ Q(x) = -EI\dfrac{d^3y}{dx^3} \end{cases} \tag{2}$$

The continuity conditions at connection points $x = -L_2$, $x = 0$, and $x = L_3$ are shown in equation (3).

$$\begin{cases} y_1(-L_3) = y_2(-L_3) \\ \theta_1(-L_3) = \theta_2(-L_3) \\ M_1(-L_3) = M_2(-L_3) \\ Q_1(-L_3) = Q_2(-L_3) \end{cases} \begin{cases} y_2(0) = y_3(0) \\ \theta_2(0) = \theta_3(0) \\ M_2(0) = M_3(0) \\ Q_2(0) = Q_3(0) \end{cases} \begin{cases} y_3(L_4) = y_4(L_4) \\ \theta_3(L_4) = \theta_4(L_4) \\ M_3(L_4) = M_4(L_4) \\ Q_3(L_4) = Q_4(L_4) \end{cases} \tag{3}$$

Using software maple to calculate, specific values of parameters A_1, A_2, B_1, B_2, C_1, C_2, D_1, D_2, E_1 and E_2 can be obtained. By using the above equation and Table 1, it becomes possible to calculate the correlation curve between the primary factors depicted in Fig. 2 and the settlement of the roof.

From Fig. 2a, the elastic modulus of the immediate roof has little effect on the control of the roof. The higher the elastic modulus of the immediate roof, the slower the speed at which the roof subsidence reaches a stable state. When the immediate roof's elastic modulus is increased from 6 GPa to 18 GPa, the peak distance from the working surface increases from 8 *m* to 10 *m*. At this point, the unfilled height is set to 1.6 *m*, and the final roof settlement value is calculated to be 1.64 *m*. This indicates that the correlation between the immediate roof elastic modulus and roof settlement is relatively small.

In accordance with Fig. 2b, set the filling height to 1.6 *m*, and when k_c increases from 0.02 to 0.3 GN/m^3. At that time, the peak value of roof settlement decreased from 2.42 *m* to 1.7 *m*. At the position close to the working face, the subsidence of the roof increases with the increase of k_c value. At the filling position, the subsidence of the roof demonstrates a negative relationship with the k_c value.

The final settlement of the roof is greatly influenced by the amount of unfilled space above the filling body, as presented in Fig. 2c. When f_c is 0.32 *m*, 0.64 *m*, 0.96 *m*, and 1.28 *m*, the respective maximum settlement values of the roof are 0.37 *m*, 0.7 *m*, 1.03 *m*, 1.36 *m*, and 1.7 *m*. It can be observed that the higher the filling height, the more effective the control over roof settlement. Therefore, when fc is controlled at a suitable position, the roof of the goaf will not experience significant settlement.

4. Model establishment

Based on the actual conditions of the CT21201 working face in Hulusu Coal Mine, a numerical simulation model is established. The middle part of the 2–1 coal seam in the Hulusu mining area is the CT21201 working face. The working face is 80 *m* wide. The coal is situated at a depth ranging from 630 *m* to 640 *m*, and it has an average height of 3.2 *m*. The model is constructed using the FLAC3D software. The model's X direction length measures 170.8 *m*, including an 80 *m* working face with 5.4 *m* wide roadways and 40 *m* wide coal pillars on both sides. The roadside support is 3 *m* wide and 3.2 *m* high, positioned adjacent to the left roadway near the goaf. There are 400 *m* in the Y direction, with a 300 *m* advance in the working face and 50 *m* coal pillars arranged on both sides. The model is 121.2 *m* high, including 20 *m* high floor, 3.2 *m* high coal seam and 98 *m* high roof. To simulate the upper strata pressure, the model's upper surface is subjected to a vertical downward load. The grid division of the 3D model is shown in Fig. 3. The stratigraphic parameters are shown in Table 2.

5. Effect of filling rate on overburden migration law in goaf

5.1. Development characteristics of overburden plastic zone in stope under different filling rates

The plastic zones' distribution under various filling rates is illustrated in Fig. 4. The filling rates are 50 %, 60 %, 70 %, 80 % and 90 % respectively, and the equivalent mining heights are 1.6 *m*, 1.28 *m*, 0.96 *m*, 0.64 *m* and 0.32 *m* respectively. When the filling rate is 50 %, as shown in Fig. 4a, the plastic zone extends into the main key stratum, the development height has expanded to about 78 *m* above the basic roof, and about 50 *m* above the working face. The plastic zone is close to the top of the model and has a continuous upward trend. When the filling rate is 60 %, as shown in Fig. 4b, there is a plastic zone distributed in the middle of the main key stratum, where the overlying rock has weakened. When the filling rate is 70 %, as shown in Fig. 4c, the plastic zone is fully developed. The plastic zone

Table 1
Value range of actors affecting roof subsidence.

Average volume force of overburden γ/(*kN* /m^3)	Elastic foundation coefficient of coal k_m/ (GN /m^3)	Elastic foundation coefficient of backfill k_c/ (GN /m^3)	Elastic modulus of immediate roof rock beam E/GPa	Height of gap between filling body and roof f_c/m
25	0.2 ~ 0.6	0.02 ~ 0.3	5 ~ 20	0.32 ~ 1.6

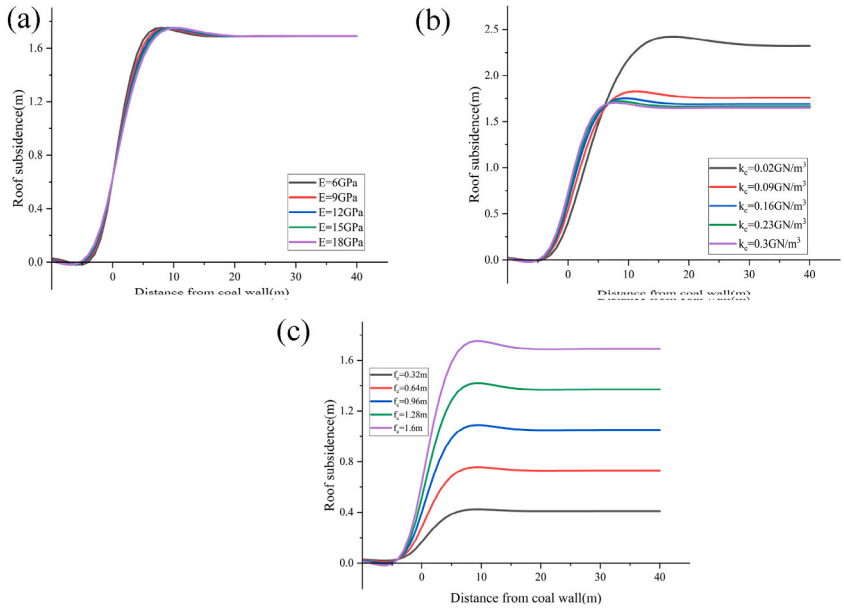

Fig. 2. Influence factors: (a) E; (b) k_c; (c) f_c.

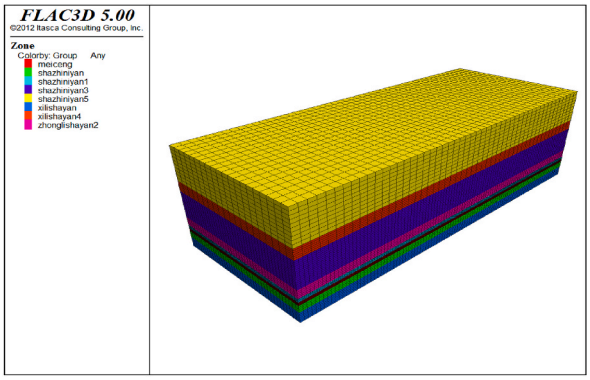

Fig. 3. Numerical simulation model.

Table 2
Physical and mechanical parameters of coal and rock strata.

Number	Rock lithology	Thickness/ m	Density/ kg • m^{-3}	Bulk modulus/ GPa	Shear modulus/ GPa	Friction angle/°	Tensile strength/MPa	Cohesion/ MPa
1	Sandy mudstone	40	2530	5.02	4.63	40	2.11	2.45
2	Siltstone	12	2468	10.26	7.39	38	1.98	2.15
3	Sandy mudstone	32	2545	5.25	6.24	36	2.14	3.02
4	Medium grained sandstone	10	2580	4.35	2.36	37	2.38	2.72
5	Sandy mudstone	4	2465	3.14	2.78	36	1.65	1.38
6	Coal	3.2	1312	0.86	0.51	25	0.62	0.18
7	Sandy mudstone	8	2590	6.56	5.03	37	2.19	2.73
8	Fine grained sandstone	12	2638	8.45	5.89	38	1.56	1.92
9	Roadside support	3.2	2480	3.76	1.97	29	1.67	1.63

develops below the key stratum, with small saddle shaped undulations, and most of the rock layers undergo shear failure, and the control of roof subsidence has achieved good results. When the filling rate is 80 %, as shown in Fig. 4d, the damage to the rock layer is relatively small, and the plastic zone is located below the key stratum, which improves the safety of mining and the stability of the

retained roadway. When the filling rate achieves 90 %, as shown in Fig. 4e, a large number of filling bodies have the best control effect on the subsidence of the overlying strata, and there will be no significant aggravation phenomenon in the working face.

5.2. Distribution law of overburden stress in stope under different filling rates

The stress distribution diagram under various filling rates of 50 %, 60 %, 70 %, 80 %, and 90 % are shown in Fig. 5a, b, Fig. 5c, d, and Fig. 5e, respectively. Table 3 displays the maximum values of the advance support pressure observed at different filling rates. The distribution of peak pressure of advanced support is shown in Table 3. As the filling rate increases, the difference in stress distribution becomes larger, and the peak pressure of advanced support decreases and gradually approaches the working face. At a filling rate of 50 %, as shown in Fig. 5a, the advance support pressure reaches a peak value of 32.17 MPa, and the peak stress point is 16.32 *m* away from the working face. As shown in Fig. 5d, when the filling rate is increased to 80 %, the peak value of advance support pressure is 27.56 MPa, which is 7.68 *m* away from the working face, the stress peak decreases by 4.61 MPa, and the distance of peak point moving closer along the working face is 8.64 *m*. As shown in Fig. 5e, when the filling rate reaches 90 %, although the high stress range at the front end of the working face decreases, the peak value of the advance support pressure increases rather than decreases compared to 80 %. In the case of high filling rate, the coal gangue waste filling body provides good support for the roof. However, the overburden stress accumulates to the coal wall at the front end of the working face and the rear end of the setup entry, causing stress concentration, which is easy to form accidents such as wall fragmentation and roof fall, and is unfavorable for the safety of the roadway.

Therefore, when the filling rate is 80 %, a good surrounding rock stress distribution can be formed, and the stability and reliability of the roadway can be improved. When the filling rate is lower than 70 %, the advance support pressure is large and has a wide influence range. When the filling rate is higher than 90 %, the advance support pressure has a small influence range but a large peak value.

5.3. Displacement characteristics of overburden in stope under different filling rates

Fig. 6(a−e) display the displacement nephogram when various filling rates are employed, and Fig. 7(a−d) show the subsidence curves of the overlying rock at different filling rates. When the filling rate is 50 %, as shown in Figs. 6a and 7(a−d), the maximum vertical displacement of overburden is 1368 mm. There are varying degrees of displacement mutations in various parts of the overlying rock, and the vertical displacement of the main key stratum is about 900 mm, which has a significant impact on the deformation of the roadway and also poses some safety hazards. When the filling rate is 60 %, as shown in Figs. 6b and 7(a−d), the maximum vertical displacement is 430 mm less than that when the filling rate is 50 %. The main key stratum has a small vertical displacement, while the sub key stratum is fractured, which is not conducive to maintaining the stability of the retained roadway. When the filling rate is 70 %, as shown in Figs. 6c and 7(a−d), the main key stratum and sub key stratum will not break, and the immediate roof and main roof will break, which will influence the stability of the retained roadway to a certain extent, but the impact is relatively small compared with the filling rate of 50 % and 60 %. When the filling rate is 80 %, as shown in Figs. 6d and 7(a−d), the roof is fractured, with a maximum

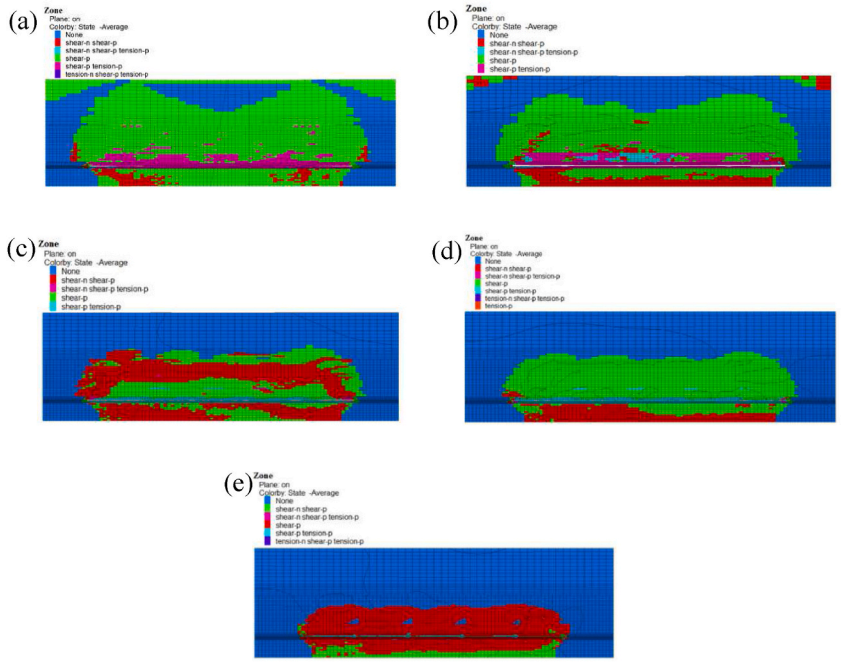

Fig. 4. Plastic zone diagram under different filling rates: (a) 50 %; (b) 60 %; (c) 70 %; (d) 80 %; (e) 90 %.

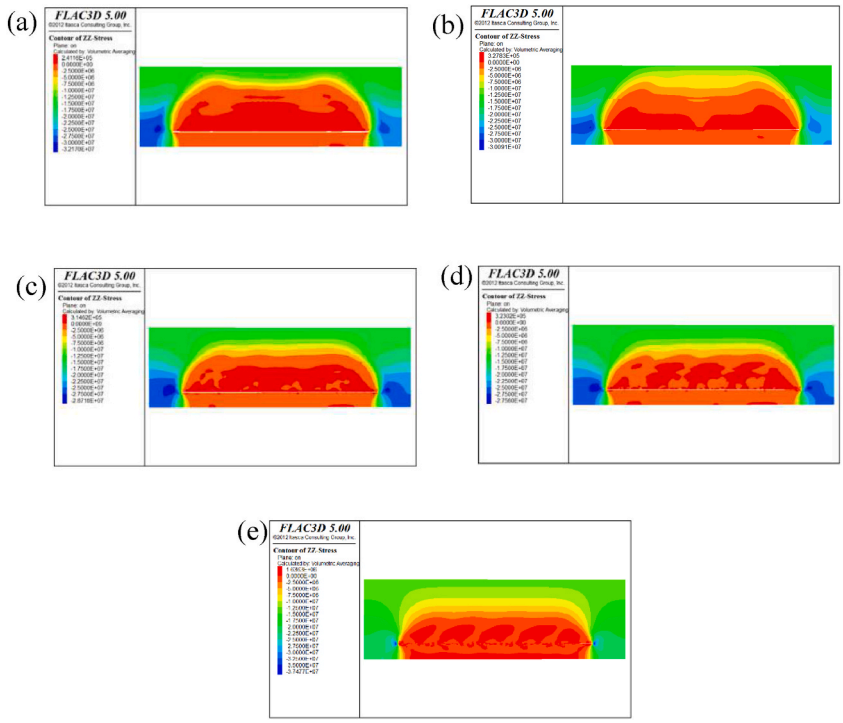

Fig. 5. Stress nephogram under different filling rates: (a) 50 %; (b) 60 %; (c) 70 %; (d) 80 %; (e) 90 %.

Table 3
Peak distribution of leading abutment pressure under different filling rates.

Filling rate/%	Maximum advance support pressure/MPa	Stress concentration factor	Distance from working face/m
50	32.17	2.04	16.32
60	30.10	1.91	13.21
70	28.72	1.82	11.35
80	27.56	1.75	7.68
90	29.48	1.85	4.08

vertical displacement of 369 mm. The basic roof failure is relatively small, and the effect of controlling overlying rock movement is good. When the filling rate is 90 %, as shown in Fig. 6e, the roof overburden subsidence can be well controlled, the main roof will not break, and the working face will not form obvious late weighting, ensuring the safety of the retained roadway as much as possible.

6. Effect of filling rate on deformation characteristics of retained roadway

6.1. Development characteristics of plastic zone of roadway retaining surrounding rock under different filling rates

When the working face advances 240 *m* and the filling rate is 70 %, the plastic zone at 40 *m* in front and behind the working face is shown in Fig. 8a and b. As shown in Fig. 8a, the plastic zone of the roof and floor of the roadway develops upwards and downwards for about 5 *m*, and the wall of the roadway develops to a depth of about 4 *m*. The main failure modes of surrounding rock are shear failure and tensile failure, with severe weakening. In Fig. 8b, the plastic zone of the roadway roof and floor develops 5 *m* upward and 4 *m* downward, and the development range of the left coal wall is about 6 *m*. The right side runs through the entire support side of the roadway and continues to develop towards the goaf, forming large-scale shear and tensile failure zones on both sides of the retained roadway.

Fig. 9a and b demonstrate the plastic zone when the filling rate is 80 % at a distance of 40 *m* in front and behind the working face. Fig. 9a reveals that the plastic zone extends 4 *m* upward along the roof, 4 *m* downward along the floor，and 4 *m* along both sides of the wall. In Fig. 9b, The development height of the plastic zone behind the working face is 4 *m*, and the development depth at the floor and coal wall is about 4 *m*, It has also runs through the goaf on the side of the roadway support body. The filling rate increment from 70 % to 80 % results in a reduction of the plastic zone to the immediate roof area.

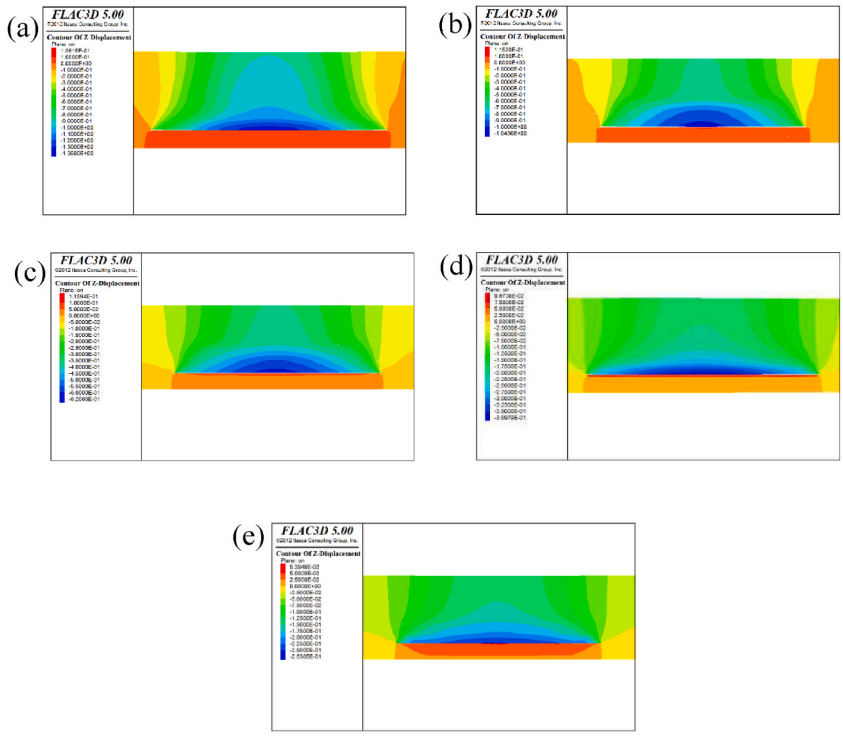

Fig. 6. Displacement nephogram under different filling rates: (a) 50 %; (b) 60 %; (c) 70 %; (d) 80 %; (e) 90 %.

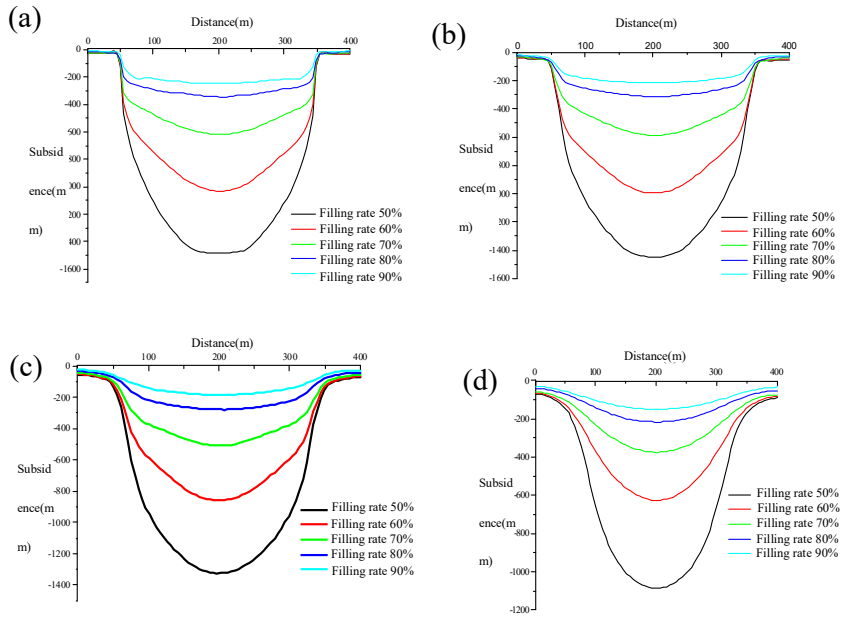

Fig. 7. Settlement curves at different locations with a filling rate of 50 %–90 %: (a) immediate roof; (b) main roof; (c) sub key stratum; (d) main key stratum.

6.2. Stress distribution characteristics of surrounding rock under different filling rates

When the working face is advanced by 240 *m* and the filling rate is 70 % and 80 %, the distribution of vertical stress at different positions on the left and right sides of the roadway in the coal seam is shown in Fig. 10a, b, 11a, 11b. As the distance from the left side of the roadway increases, the vertical stress along the coal seam gradually decreases until it approaches the original rock stress. When

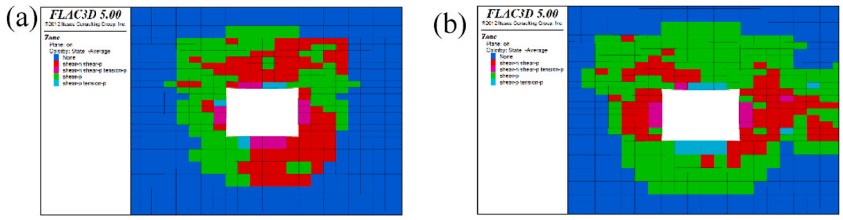

Fig. 8. Distribution diagram of plastic zone under 70 % filling rate: (a) 40 *m* in front of the working face; (b) 40 *m* behind the working face.

the distance from the left side of the roadway is 5 *m*, a peak stress occurs. Compared with a 70 % filling rate, the lower the stress at 80 % filling rate, the better the stress distribution. On the right side of the roadway, the stress in the leading working face continuously decreases towards the goaf side. On the side of the goaf, it gradually increases from the right side of the retained roadway to the goaf side, and the increase and decrease of both tend to stabilize at a distance of 20 *m* from the right side of the retained roadway. Compared with the 70 % filling rate, when the filling rate is 80 %, the stress value at the same position of the goaf on the right side of the retained roadway is greater, so an 80 % filling rate can form better support for the roof.

6.3. Deformation law of retained roadway under different filling rates

In Fig. 12a and b, the surface deformation of the retained roadway under the condition of 80 % filling rate is less than that under the condition of 70 % filling rate. The area with the greatest deformation in the remaining roadway occurs at the roof of the roadway, followed by the two sides of the roadway, and the area with the smallest deformation is the floor of the roadway. In addition, the deformation patterns of the roof and sides of the retained roadway are similar. The deformation of the roof and edge is continuously decreasing and stabilizing along the advancing direction of the working face, and tends to stabilize at 10–20 *m* ahead of the working face. The deformation along the goaf direction from the working face first increases and then tends to stabilize, and tends to stabilize at a distance of 30–50 *m* behind the working face. The deformation of the floor is close to a straight line. After analysis, the first reason is that the floor itself has good physical and mechanical properties. Secondly, considering the fact that the working face is 80 *m* and relatively short, as well as factors such as goaf filling, these factors to some extent weaken the rock pressure of the floor and reduce the deformation of the floor. Under the conditions of 70 % and 80 % different filling rates, when the working face was advanced by 240 *m*, the evolution law of the surface displacement of the retained roadway at different positions in front of and behind the working face is analysed. When the filling rate is 80 %, the surface deformation and deformation gradient of each part of the roadway are smaller than when the filling rate is 70 %. From the angle of roadway deformation, it is revealed that 80 % filling rate can effectively control roadway deformation and improve the stability of roadway.

7. Discussion and conclusion

7.1. Discussion

By establishing a mechanical model, the influence of factors such as the elastic modulus and filling rate of the immediate roof on the subsidence of the roof was analysed. The subsidence of the roof is mainly controlled by the filling rate, with little influence from changes in the elastic modulus of the immediate roof and the elastic foundation coefficient of the filling body. When f_c is 0.32 *m*, 0.64 *m*, 0.96 *m*, 1.28 *m*, and 1.6 *m*, the roof's maximum subsidence values are 0.37 *m*, 0.7 *m*, 1.03 *m*, 1.36 *m*, and 1.7 *m*. It is evident that a higher filling rate leads to improved roof control, thereby achieving the objective of ensuring roof safety.

Through a comprehensive analysis of the development characteristics, vertical stress field, and displacement field evolution of the plastic zone under the conditions of 50 %, 60 %, 70 %, 80 %, and 90 % filling rates, it is believed that when the filling rate reaches 70 % or above, the roof control effect is good. However, when the filling rate reaches 90 % or above, the peak value of advanced support stress increases sharply. Further analysis was conducted on the safety of the roadway when the filling rate was 70 % and 80 %, and it was found that when the filling rate was 80 %, the development range of the plastic zone and peak stress around the roadway was smaller than when the filling rate was 70 %.

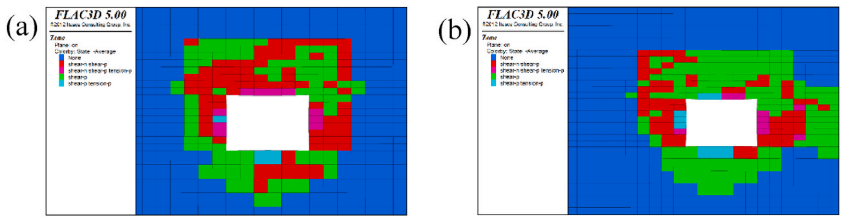

Fig. 9. Distribution diagram of plastic zone under 80 % filling rate: (a) 40 *m* in front of the working face; (b) 40 *m* behind the working face.

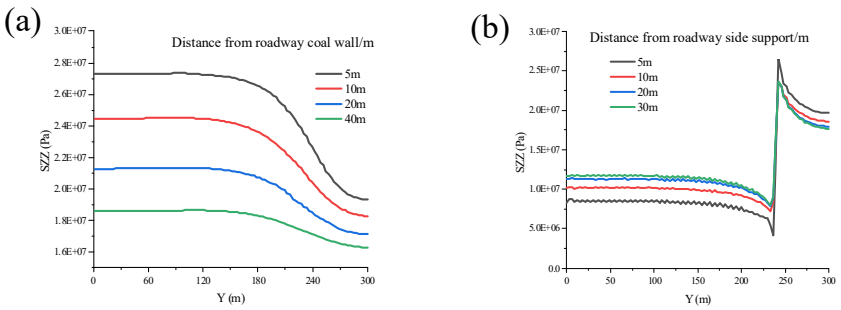

Fig. 10. Vertical stress curve at a filling rate of 70 %: (a) Coal wall side; (b) Goaf side.

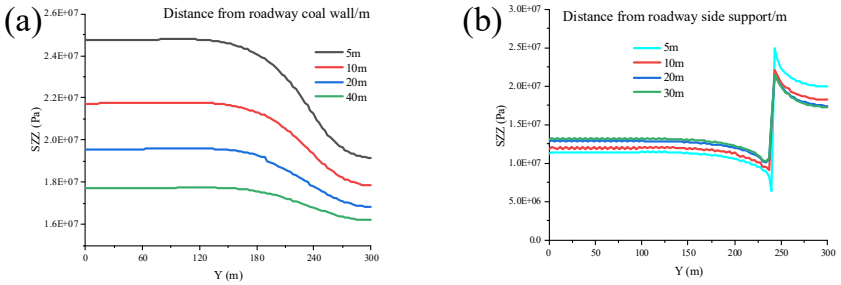

Fig. 11. Vertical stress curve at a filling rate of 80 %:(a) Coal wall side; (b) Goaf side.

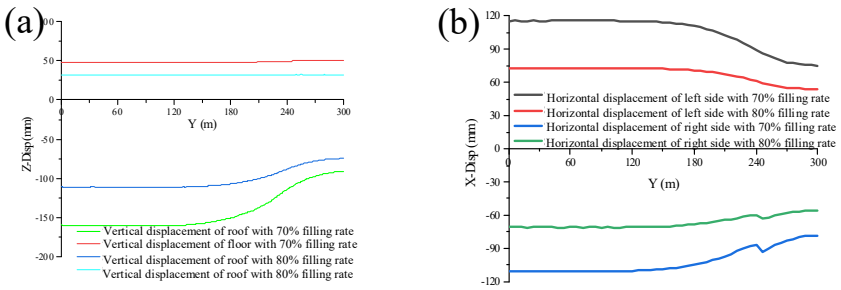

Fig. 12. Deformation diagram of retained roadway at 70 % and 80 % filling rates: (a) the roof and floor of the roadway; (b) the side walls of the roadway.

7.2. Conclusion

Taking the CT21201 working face of Hulusu Coal Mine as the engineering background, the influence of filling rate on the migration law of surrounding rock in the mining area and retained roadway is analysed. The conclusion is as follows.

(1) The analysis of the influence curve of factors such as the elastic modulus of the immediate roof and filling rate on roof subsidence shows that filling rate is the main control factor for roof settlement, while other factors have little impact on roof settlement.
(2) When the filling rate is between 70 % and 80 %, stress distribution, the plastic zone failure range, and roof subsidence in the mining area are well controlled, improving the continuity and stability of the overlying rock layer, and ensuring the safety of the retained roadway.
(3) Compared with a filling rate of 70 %, a plastic zone with an 80 % filling rate has a smaller development range and can be effectively controlled in the immediate roof area. When the filling rate is 80 %, compared to 70 %, the stress value decreases and the stress distribution state is better. The deformation of each part of the retained roadway at 80 % filling rate is less than 70 %. It indicates that an 80 % filling rate is more favorable for the stability control of the roadway.

Funding

Project U22A20165, 52,174,089, 52,104,106 supported by National Natural Science Foundation of China, Supported by State Key Laboratory of Green and Low-carbon Development of Tar-rich Coal in Western China, Xi'an University of Science and Technology, SKLCRKF21-08.

Data availability

Data included in article/supp. Material/referenced in article. The Microsoft Excel Worksheet data used to support the findings of this study are available from the corresponding author upon request.

CRediT authorship contribution statement

Kai Sun: Writing – original draft. **Yongjin Huo:** Writing – review & editing. **Jian Li:** Methodology. **Fei Guo:** Data curation, Investigation. **Yinghao Hao:** Data curation, Formal analysis. **Gang Bai:** Data curation, Investigation. **Yuyi Wu:** Data curation, Formal analysis. **Xiaofang Wo:** Data curation.

Declaration of competing interest

The authors declare that they have no known competing financial interests or personal relationships that could have appeared to influence the work reported in this paper.

References

[1] D.Y. Fan, X.S. Liu, Y.L. Tan, L. Yan, S.L. Song, J.G. Ning, An innovative approach for gob-side entry retaining in deep coal mines: a case study, Energy Sci. Eng. 7 (6) (2019) 2321–2335.
[2] G.R. Feng, P.F. Wang, Y.P. Chugh, A new gob-side entry layout for longwall top coal caving, Energies 11 (5) (2018) 24.
[3] G. Li, J. Li, Y. Sun, C. Sun, J. Xu, H. Rong, S. Yang, X. Wo, Z. Lu, Advance of multi-scale study on both analytic models and water-rock interaction characteristics of mudstone, Meitan Xuebao/J. China Coal Soc. 47 (3) (2022) 1138–1154.
[4] Y. Sun, G. Li, D. Qian, S. Zhang, J. Xu, Research and application of BAS-ESVM model for rheological parameter inversion of soft coal mass in roadway, Meitan Xuebao/J. China Coal Soc. 46 (2021) 106–115.
[5] K. Wang, B.G. Yang, P.Y. Wang, C. Li, Deformation and failure characteristics of gob-side entry retaining in soft and thick coal seam and the control technology, Rock Soil Mech. 43 (7) (2022) 1913–+.
[6] X.S. Shi, H.W. Jing, Z.L. Zhao, Y. Gao, Y.C. Zhang, R.D. Bu, Physical experiment and numerical modeling on the failure mechanism of gob-side entry driven in thick coal seam, Energies 13 (20) (2020) 24.
[7] Y.T. Sun, R.Y. Bi, J.B. Sun, J.F. Zhang, R. Taherdangkoo, J.D. Huang, G.C. Li, Stability of roadway along hard roof goaf by stress relief technique in deep mines: a theoretical, numerical and field study, Geomech. Geophys. Geo-Energy Geo-Resour. 8 (2) (2022) 16.
[8] X. Liu, S.H. Tu, D.Y. Hao, Y.D. Lu, K.J. Miao, W.L. Li, Deformation law and control measures of gob-side entry filled with gangue in deep gobs: a case study, Adv. Mater. Sci. Eng. 2021 (2021) 13.
[9] T. Li, G.B. Chen, Z.C. Qin, Q.H. Li, B. Cao, Y.L. Liu, The gob-side entry retaining with the high-water filling material in Xin'an Coal Mine, Geomech. Eng. 22 (6) (2020) 541–552.
[10] Z.Z. Zhang, X.Y. Yu, H. Wu, M. Deng, Stability control for gob-side entry retaining with supercritical retained entry width in thick coal seam longwall mining, Energies 12 (7) (2019) 16.
[11] C. Li, Y. Liu, J. Bai, Q. Ge, Study on stability of filling wall under lateral large-span composite hinge fracture of hard critical block, Sci. Prog. 104 (2) (2021), 368504211021694.
[12] W.T. Liu, L.F. Pang, Y.B. Liu, Y.H. Du, Characteristics analysis of roof overburden fracture in thick coal seam in deep mining and engineering application of super high water material in backfill mining, Geotech. Geol. Eng. 37 (4) (2019) 2485–2494.
[13] X.B. Li, D.Y. Wang, C.J. Li, Z.X. Liu, Numerical simulation of surface subsidence and backfill material movement induced by underground mining, Adv. Civ. Eng. 2019 (2019) 17.
[14] N. Abbas, W. Shatanawi, Heat and mass transfer of micropolar-casson nanofluid over vertical variable stretching riga sheet, Energies 15 (14) (2022) 20.
[15] N. Abbas, W. Shatanawi, F. Hasan, T.A.M. Shatnawi, Numerical analysis of Darcy resistant Sutterby nanofluid flow with effect of radiation and chemical reaction over stretching cylinder: induced magnetic field, AIMS Math 8 (5) (2023) 11202–11220.
[16] S.R. Xie, H. Pan, D.D. Chen, J.C. Zeng, H.Z. Song, Q. Cheng, H.B. Xiao, Z.Q. Yan, Y.H. Li, Stability analysis of integral load-bearing structure of surrounding rock of gob-side entry retention with flexible concrete formwork, Tunn. Undergr. Space Technol. 103 (2020) 11.
[17] G.C. Li, Y.T. Sun, C.C. Qi, Machine learning-based constitutive models for cement-grouted coal specimens under shearing, Int. J. Min. Sci. Technol. 31 (5) (2021) 813–823.
[18] J.Z. Li, Z.Q. Yin, Y. Li, C.M. Li, Waste rock filling in fully mechanized coal mining for goaf-side entry retaining in thin coal seam, Arabian J. Geosci. 12 (16) (2019) 11.
[19] A. Nazir, N. Abbas, W. Shatanawi, On stability analysis of a mathematical model of a society confronting with internal extremism, Int. J. Mod. Phys. B 37 (7) (2023) 13.
[20] Q.Y. Shan, Y.L. Liu, T. Li, Z.P. Jin, Asymmetric support technology for gob side entry retaining with high water material, Acta Geodyn. Geomater. 18 (3) (2021) 335–346.
[21] Q.L. Chang, W.J. Tang, Y. Xu, H.Q. Zhou, Research on the width of filling body in gob-side entry retaining with high-water materials, Int. J. Min. Sci. Technol. 28 (3) (2018) 519–524.
[22] C.W. Hu, E.Y. Wang, Q. Li, Y.L. Wang, Y.Y. Li, X.F. Sha, Research on the key technology of gob-side entry retaining by roof cutting for thick and hard sandstone roofs, Sustainability 14 (16) (2022) 14.
[23] D.D. Pang, Y. Zhou, X.G. Niu, K. He, C.M. Li, Z.Q. Chen, Research on the mechanical properties of flexible material backfilling wall in gob-side entry retaining, Minerals 12 (8) (2022) 15.
[24] E.Z. Zhen, Y.J. Wang, J. Yang, M.C. He, Comparison of the macroscopical stress field distribution characteristics between a novel non-pillar mining technique and two other current methods, Adv. Mech. Eng. 11 (5) (2019) 15.
[25] H.Y. Liu, B.Y. Zhang, X.L. Li, C.W. Liu, C. Wang, F. Wang, D.Y. Chen, Research on roof damage mechanism and control technology of gob-side entry retaining under close distance gob, Eng. Fail. Anal. 138 (2022) 16.

[26] N. Abbas, W. Shatanawi, T.A.M. Shatnawi, F. Hasan, Theoretical analysis of induced MILD Sutterby fluid flow with variable thermal conductivity and thermal slip over a stretching cylinder, AIMS Math 8 (5) (2023) 10146–10159.
[27] W.X. Zheng, H.Q. Duan, Discussion on stability analysis and support technology of surrounding rock of gob-side entry retaining, J. Vibroeng. 21 (4) (2019) 1058–1068.
[28] Y.T. Sun, R.Y. Bi, Q.L. Chang, R. Taherdangkoo, J.F. Zhang, J.B. Sun, J.D. Huang, G.C. Li, Stability analysis of roadway groups under multi-mining disturbances, Appl. Sci.-Basel 11 (17) (2021) 17.
[29] P. Wang, L. Ding, Y.J. Ma, T. Feng, G.J. Sun, Y.J. Zhu, H. Ren, P. Li, Y.Q. Zhang, X.Z. Wang, A case study on gob-side entry retaining technology in the deep coal mine of xinjulong, China, Adv. Civ. Eng. 2020 (2020) 10.
[30] Z.Q. Wang, J. Zhang, J.K. Li, P. Wang, C. Wu, L. Shi, Research of surrounding rock control of gob-side entry retaining based on deviatoric stress distribution characteristics, Sustainability 14 (9) (2022) 21.
[31] Z.M. Ma, Z.B. Guo, H.H. Wang, J.Z. Hu, T. Li, J. Chen, Large deformation mechanism and three-level control technology of entry retaining in three-soft thick coal seams, Geotech. Geol. Eng. 38 (6) (2020) 6125–6143.